Research Article Vol. 31, No. 3 / 30 Jan 2023 / Optics Express 3676

Optics EXPRESS

Speed-up coherent Ising machine with a spiking neural network

BO LU,[1] CHEN-RUI FAN,[1] LU LIU,[1] KAI WEN,[2] AND CHUAN WANG[1,3,*]

[1] *School of Artificial Intelligence, Beijing Normal University, Beijing 100875, China*
[2] *Beijing QBoson Quantum Technology Co., Ltd., Beijing 100015, China*
[3] *Applied Optics Beijing Area Major Laboratory, Beijing Normal University, Beijing 100875, China*
[*] *wangchuan@bnu.edu.cn*

Abstract: Coherent Ising machine (CIM) is a hardware solver that simulates the Ising model and finds optimal solutions to combinatorial optimization problems. However, for practical tasks, the computational process may be trapped in local minima, which is a key challenge for CIM. In this work, we design a CIM structure with a spiking neural network by adding dissipative pulses, which are anti-symmetrically coupled to the degenerate optical parametric oscillator pulses in CIM with a measurement feedback system. We find that the unstable oscillatory region of the spiking neural network could assist the CIM to escape from the trapped local minima. Moreover, we show that the machine has a different search mechanism than CIM, which can achieve a higher solution success probability and speed-up effect.

1. Introduction

With the stagnation of Moore's Law and the high power consumption of the von Neumann architecture, there is a huge demand for higher performance of computational power which requires us to find new computing methods. Recently progress in optical and quantum computing is paving the way for new paradigms in computing. Among these different methods, the coherent Ising machine (CIM) is a promising approach that is proposed recently to solve the combinatorial optimization problem by mapping its cost function to the search of the ground state in the Ising model [1,2].

A typical CIM machine uses the bistable interfering of the coupled optical state to find the optical configuration of the ground state through the principle of minimum gain which corresponds to the solution of the problem [3–6]. The hardware solver is different from traditional von Neumann computational structures and will be of high significance [7–9]. Compared with different non-Von Neumann architectures, the CIMs have attracted much attention for their excellent computing performance [10]. During the past decades, it has been implemented in various physical systems, such as optical system [5,6,11,12], nanomagnetic-net arrays [13,14], single-atom [15] and complementary oxide semiconductor devices [16]. Meanwhile, it has exhibited significant implications for finance, logistics, drug design, and machine learning.

Traditionally, the proposed optical CIMs are mainly based on the degenerate optical parametric oscillations (DOPO), which uses phase-sensitively amplified optical pulses to represent the binary spins of the Ising model [17]. Recently, it has been widely studied due to its fully connected programmable and scalable [18,19]. In addition, CIM based on DOPO has been applied to graph clustering [20], coloring problems [21], and communication resource allocation [22,23]. However, the energy evolution of the system may be trapped in the local minima and the interference of the coherent optical states is phase-sensitive, thus making the CIM computation technically challenging [24,25]. In the DOPO-based CIMs, the amplitude error correction signals are introduced as a solution to reduce these problems [25–28].

#479903 https://doi.org/10.1364/OE.479903
Journal © 2023 Received 3 Nov 2022; revised 13 Dec 2022; accepted 23 Dec 2022; published 17 Jan 2023

Optics EXPRESS

Recently, the spiking neurons are regarded as the next generation of computational neural networks [29–31], and their brain-like learning characteristics have also been studied [32,33]. Experiments on spiking neural networks (SNN) simulated by DOPO-based CIM demonstrate the complex cluster synchronization phenomenon [34], and CIM with SNN exhibits excellent computational performance on combinatorial optimization problems [35]. In this study, by combining the SNN with CIM, we propose a new structure of CIM with SNN by coupling the dissipative pulses anti-symmetrically to the DOPO pulses in CIM with a measurement feedback scheme. Exploiting the Gaussian homodyne measurement theory [36], the performance of SNN-based CIM by the quantum noise is also studied. Moreover, we demonstrate the dynamics of SNN-CIM under the increasing pump which shows that the unstable oscillations in SNN-based CIM can be used to escape the solutions from trapped local minima. In addition, the computational performance of problems with different scales is also studied, which reveals that SNN-based CIM has a higher probability of finding successful solutions and speed-up effect compared with the conventional CIMs.

2. Model of SNN-based CIM

The key component of the CIM is the ensemble of binary optical spins, and the interaction of the spins could be achieved by the coupling of the optical pulses. As shown in Fig. 1(a), the measurement-feedback (MFB) is employed to achieve the feedback coupling which may improve the performance of CIM in solving combinatorial optimization problems [5,6,10]. Specifically, the CIM with MFB expresses the amplitude parametric amplified pulses generated by DOPO as the analog spins, denoted as μ-type pulses. A small part of each pulse is split for homodyne detection, and the amplitude of the pulse is measured each round in the fiber-ring cavity. The measurement results of the amplitude μ_i of i-th pulse are calculated in the FPGA as a feedback pulse and injected into the fiber-ring cavity of the main optical path again through the coupler (with reflectance $R_B \ll 1$).

Here, the time evolution of the amplitude μ_i of i-th pulse can be written as $d\mu_i/dt = -\partial V(\mu_i)/\partial\mu_i = -\mu_i + p\mu_i + g^2\mu_i^3 - \sum_{i'} J_{ii'}\mu_{i'}$. In this equation, the first, second, and third terms represent the normalized loss, linear gain pump rate p, and nonlinear saturation rate g^2, respectively. The last coupling term could be mapped to the Ising model $H = -\frac{1}{2}\sum_{ij} J_{ij}\sigma_i\sigma_j$. The dynamics of bifurcation of the potential function $V(\mu_i) = \frac{\mu_i^2}{2}(1-p) + g^2\frac{\mu_i^4}{4} + \sum_{i'} J_{ii'}\mu_i\mu_{i'}$ under different pumps is shown in Fig. 1(b). We notice that the pulse amplitude is not amplified for a small pump, and $V(\mu_i)$ becomes a paradigmatic bistable potential when the pump is above the threshold, where the collective symmetry breaking brings the spins into the lower-energy states (with positive or negative amplitude, corresponding to the spins either in the spin-up state or in the spin-down state). However, compared with the Ising model of binary spins, the variation of $V(\mu_i)$ result in different times for different spins to reach stability and amplitude heterogeneity during stabilization. This may reduce the computational performance of CIM on combinatorial optimization problems [24,26,27].

To further eliminate the influence of the above effect, we design an SNN-based CIM by injecting b-type dissipative pulse that is anti-symmetrically coupled to each μ-type pulse ($J_{\mu b} = -J_{b\mu} = 1$) in the fiber-loop of the CIM with MFB. A schematic diagram of the model by the optical implementation is shown in Fig. 1(a). The dissipative pulse b can be directly injected through the propagation of the pulses along the optical loop when the pump is turned off, and the linear dissipation is regulated by the MFB system.

In a typical DOPO process, second-order nonlinear interaction $\chi^{(2)}$ with strength κ occurs between the pump mode $\hat{a}_p$ and the signal mode $\hat{a}_s$, considering dissipative pulse signal coupling and the interaction Hamiltonian could be described by $\hat{H}_{int} = i\hbar\kappa(\hat{a}_s^{\dagger 2}\hat{a}_p - \hat{a}_p^{\dagger}\hat{a}_s^2) + i\hbar\gamma_b b(\hat{a}_s - \hat{a}_s^{\dagger})$,

Optics EXPRESS

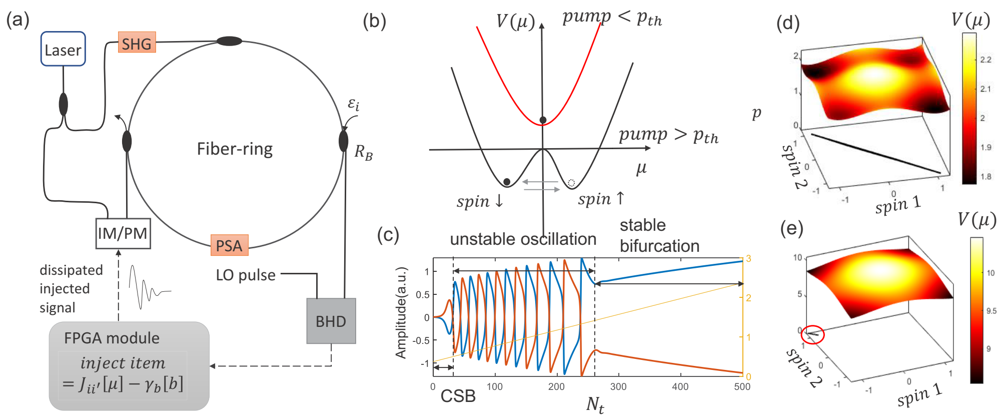

Fig. 1. A schematic diagram of the SNN-based CIM and the dynamical evolution in coherent computing. (a) A schematic diagram of the model by the optical implementation. SHG, second harmonic generation; FPGA, field-programmable gate array, PSA, phase-sensitive amplification; IM/PM, intensity/phase modulator; BHD, balanced homodyne detection. (b) The potential function $V(\mu)$ does not oscillate when the pump is below the oscillation threshold (red curves) and becomes the bistable potential above the threshold (black curves). (c) Evolution of the analog spin parametric amplification amplitude with increasing the pump in antiferromagnetically coupled SNN-based CIM. CSB: collective symmetry breaking. (d) and (e) correspond to the potential energy $V(\mu)$ distribution and spin trajectory evolution (black curves) in the initial stage of evolution (N_t<150) and the stable stage (N_t>400) in (b).

where γ_b is the linear loss intensity modulated by MFB. This interaction Hamiltonian could be written as the Fock-Planck equations of the positive-p distribution function [37], and the equivalent c-number statistical differential equations (SDEs) can be obtained by ignoring the higher-order terms [38,39]. The equivalent c-number SDEs of signal mode a_s are

$$\frac{da_s}{dt} = -a_s + pa_s^{\dagger} - g^2 a_s^{\dagger} a_s^2 - \gamma_b b + \sqrt{p - g^2 a_s^2}\varepsilon_1, \tag{1}$$

$$\frac{db}{dt} = -\gamma_b b + a_s. \tag{2}$$

Here, ε_j is the real random variable satisfying $\langle \varepsilon_j(t)\varepsilon_{j'}(t')\rangle = \delta_{jj'}\delta(t-t')$. We denote the $a_s = \langle a_s\rangle + \Delta a_s$ and the quantum fluctuations satisfy $m = \langle \Delta a_s^2\rangle$ and $n = \left\langle \Delta a_s^{\dagger}\Delta a_s\right\rangle$. Using Gaussian homodyne measurement theory and by considering the injecting terms [36,40,41], the mean amplitude $\mu = \langle a_s\rangle$, dissipative pulse amplitude b, and variances of quantum fluctuations $n(m)$ of the SNN-CIM model can be expressed as

$$\begin{aligned}\tfrac{d\mu_i}{dt} &= -(1-p+j)\mu_i - g^2(\mu_i^2 + 2n_i + m_i)\mu_i + \sqrt{j}(n_i+m_i)W_i \\ &+ j\sum_{i'} J_{ii'}(\mu_{i'} + W_{i'}/\sqrt{4j}) - j\gamma_b b,\end{aligned} \tag{3}$$

$$\frac{db_i}{dt} = -\gamma_b b + j(\mu_i + W_i/\sqrt{4j}), \tag{4}$$

$$\begin{aligned}\tfrac{dn_i}{dt} &= -2(1+j)n_i + 2pm_i - 2g^2\mu_i^2(2n_i+m_i)\mu_i \\ &- j(m_i+n_i)^2,\end{aligned} \tag{5}$$

$$\frac{dm_i}{dt} = -2(1+j)m_i + 2pn_i - 2g^2\mu_i^2(2m_i+n_i)\mu_i + p \\ -g^2(\mu_i^2+m_i) - j(m_i+n_i)^2. \tag{6}$$

Here $j = R_B/\Delta t$ denotes the linear dissipation rate due to the measurement of injection coupling and W_i represents a random real value of normally distributed vacuum noise.

3. Dynamical behaviors of the SNN-CIM

In the following, we study the dynamical behaviors of the SNN-based CIM by numerical simulations. Here we choose an antiferromagnetically coupled two-spin Ising problem ($J = -1$) as an example, which is apparently stable in a state where the two spins have the opposite spin directions. We start with a small pump that increases linearly in order to satisfy the minimum gain principle [4]. The time step is set as $\Delta_t = 0.05$ and the saturation parameter $g^2 = 0.01$ as shown in Fig. 1(c)-(e). It is obvious that the mean amplitude evolution can be divided into three stages as shown in Fig. 1(c). The first stage describes the evolution from noisy conditions to collective symmetry breaking, and the third stage is the stable bifurcation, which is the same as the bifurcation process of CIM. Due to the effect of the dissipative pulses, SNN-based CIM has a unique stage of unstable oscillation compared to CIM, and this dynamic behavior from oscillation to stability with the addition of pump increases similar to class-II neurons with Andronov-Hopf (AH) bifurcation [42]. The relationship between the amplitude trajectory of the spins and the potential function $V(\mu)$ is shown in Fig. 1(d) and (e). Compared with the CIM bifurcation that the transition between spin $\downarrow$ state and the spin $\uparrow$ state cannot occur due to the potential barrier, the unstable oscillation of SNN-based CIM can help the spin state to cross the potential barrier to achieving the transition, as shown by black curves in Fig. 1(d) and the gray curves in Fig. 1(b). Finally, we find the SNN-based CIM presents a stable state in the stable bifurcation phase, such as $|\downarrow\uparrow\rangle$ in Fig. 1(e).

Moreover, we compare the dynamical behaviors of SNN-based CIM with the dynamic process of the antiferromagnetic two-spin Ising model solved by the CIM model. The minimum gain of the system is increased due to the effect of the dissipative pulses, and the coupling strength of SNN-based CIM is slightly larger than that of CIM $J_S = 3J_C$. They are both driven by the same pumping power $p = 1 + tanh(0.1(t+2))$, and other parameters are $\Delta t = 0.002$, $j = 2$, and $g^2 = 10^{-3}$ as shown in Fig. 2. In Fig. 2(b), we find the variance $\langle \Delta X_i^2 \rangle = n_i + m_i + \frac{1}{2}$ is anti-squeezed while the variance $\langle \Delta P_i^2 \rangle = n_i - m_i + \frac{1}{2}$ is squeezed in the CIM model. In the trajectory of variance in Fig. 2(c), the DOPO state evolves from a coherent state that satisfies the minimum uncertainty product $\langle \Delta X_i^2 \rangle \langle \Delta P_i^2 \rangle = 1/4$ to a squeezed vacuum state, and the whole process is in a parametric amplification process. However, under the dynamics of SNN-based CIM, the trajectory of variance has both parametric amplification and parametric de-amplification. As a result of this alternate search, the system finally stabilizes in a coherent state with the minimum uncertainty product. This differs from CIM, where the uncertainty product is much greater than 1/4.

In order to study SNN-CIM and CIM with multi-node networks, a classical combinatorial optimization problem, the Max-Cut problem with nodes N=25, is used to study the computational performance of the model. The graph to be solved for the Max-Cut problem is randomly generated. We choose the problem scale $N = 25$, edge density $d = E/N = 3$, which contains 75 edges, and try to make each node have 3 edges. The purpose of the Max-Cut problem is to divide the vertices of a graph into two types with as many edges being cut as possible, which is generally considered to be equivalent to the Ising model as

$$edges = \frac{1}{4}(\sum_{ij} J_{ij} - \sum_{ij} J_{ij}\sigma_i\sigma_j). \tag{7}$$

Here $\sum_{ij} J_{ij}\sigma_i\sigma_j$ corresponds to the lowest energy of the Ising model. The problem graph, the

Optics EXPRESS

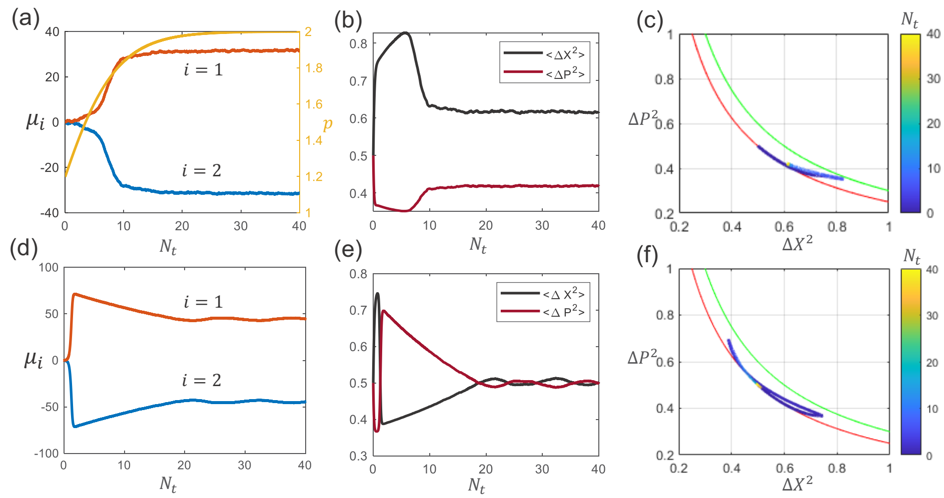

Fig. 2. Dynamics in SNN-based CIM and CIM. (a), (b) The evolution of mean amplitude (μ_i) and variances ($\langle \Delta X^2 \rangle$, $\langle \Delta P^2 \rangle$) of the antiferromagnetic two-spin in CIM with the increasing pump. (c) The trajectory of the variance ($\langle \Delta X^2 \rangle$, $\langle \Delta P^2 \rangle$) during the computation. (d) to (f) correspond to the results for SNN-based CIM.

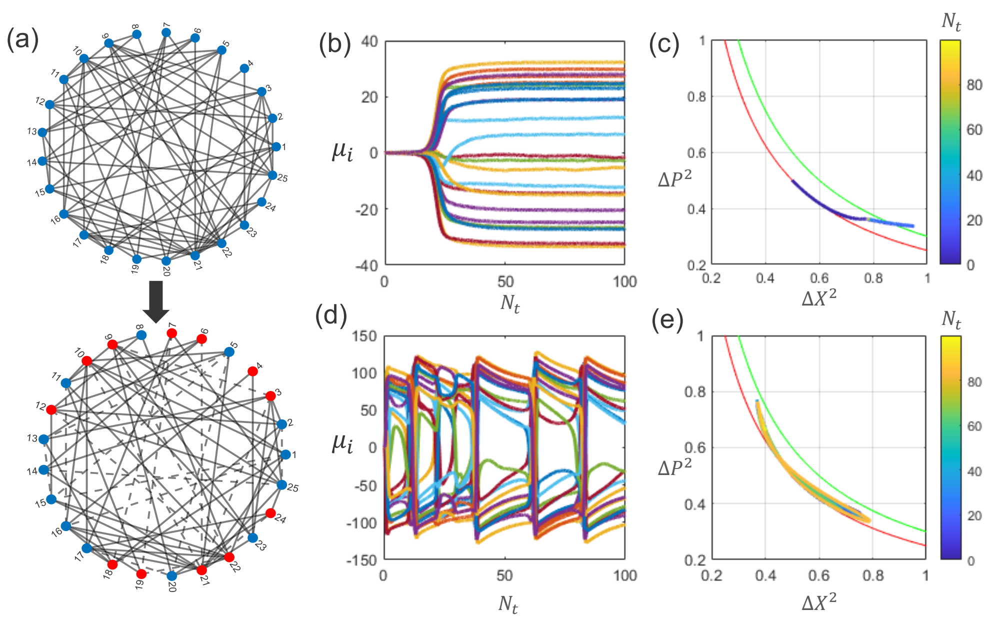

Fig. 3. The dynamics of CIM and SNN-based CIM in solving the Max-Cut problem. (a) A randomly generated example graph (top, *node* = 25 and *edge* = 75) and one of its maximum cuts obtained by solving it (bottom). The red dots (blue dots) represent $\sigma_i = 1$ ($\sigma_i = -1$), and the dashed lines represent edges that were not counted towards the maximum cut number during the cut. (b), (c) The evolution of mean amplitude (μ_i) and variances trajectory ($\langle \Delta X^2 \rangle$, $\langle \Delta P^2 \rangle$) of the Ising model corresponding to (a). (d), (e) correspond to the results for SNN-based CIM.

solution of the problem, and the evolution results of the two models are given in Fig. 3. The best solutions could be solved by both the two models, and the dynamic process is similar to the case of the two spins above. The unstable oscillation in Fig. 3(d) is because the pump rate has not approached the stable bifurcation. However, the Ising model under the corresponding spins configuration of the system has reached the lowest energy and is kept stable.

4. Comparison of the performance between SNN-based CIM and CIM

In order to compare the effect of the dissipative pulse b in the SNN-based CIM, we numerically studied the success rates of different γ_b in solving the Max-Cut problem with N=25 nodes. The problem is run 100 times, and the optimal solution could be obtained within the running time N_t as a successful solution, and the result is shown in Fig. 4(a). Compared with the conventional CIM, in which γ_b is equal to zero, a larger γ_b can help the system to find the optimal solution with a greater probability. Moreover, the curve of probability approaches the maximum value earlier, which speeds up the calculation of the system.

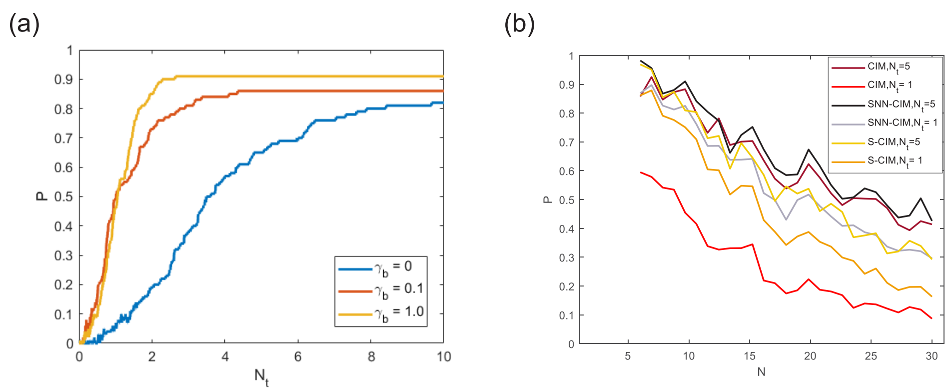

Fig. 4. The speed-up performance of SNN-based CIM relative to CIM and S-CIM. (a) Dissipative rate γ_b versus probability of success, on the Max-Cut problem with $N = 25$ and computation time $N_t = 10$. (b) The relationship between success rate and problem size. Generate 50 random graphs under each N, and each graph was solved 50 times to obtain a statistical average success rate. The other parameters are $j = 2$, $\Delta t = 0.002$, $\gamma_b = 0.1$ and $g^2 = 0.1$.

Further to study the computational performance of SNN-based CIM and CIM on different scale problems, we generate 50 random graphs at each problem size. And each graph is solved by 100 times to obtain the average success rate. The randomly generated graph is a fully connected graph, and the edge weights w_{ij} is randomly selected from 21 discrete values from -1 to 1, $w_{ij} \in \{-1, -0.9, -0.8, \ldots, 0.8, 0.9, 1\}$. The average solution of the success rates curves for different problem sizes N at solution times $N_t = 1$ and $N_t = 5$ are shown by Fig. 4(b). The variation of the solution successful rate of SNN-based CIM under different problem scales is similar to that of CIM while showing slightly higher than that of CIM. Moreover, comparing the success rate curve $N_t = 1$ with $N_t = 5$, it can be clearly found that the speed-up calculation of SNN-based CIM relative to CIM and S-CIM (CIM optimized by sigmoid function [43]).

The saturation parameter g^2 represents the inverse process of converting two signal photons into a pump photon under nonlinear effects. It has been shown that the intensity of this process affects the success rate of CIM [27,44]. Here we solve the small-scale and medium-scale problems 100 times to obtain the effect of saturation parameters on the solution success rate, and the results are shown in Fig. 5. For CIM, a slightly increased g^2 can improve the success rate, while when g^2 approaches 1, a huge saturation parameter will drastically decrease the solution success rate.

Optics EXPRESS

However, the solution success probability of SNN-based CIM is less affected by a large saturation parameter. The reason may be that the increase of the nonlinear saturation term affected by g^2 in CIM will lead to the intensification of amplitude heterogeneity, and the SNN-based CIM constantly switches between amplitude amplification and amplitude de-amplification during the solution, which may weaken the effect of g^2.

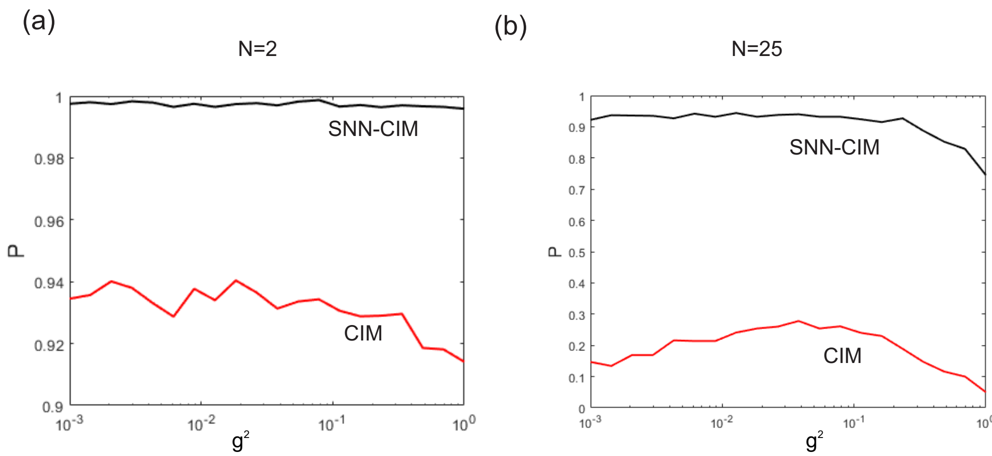

Fig. 5. The effects of saturation parameter g^2 on the success rate of the CIM algorithm. (a) is $N = 2$ and (b) is $N = 25$. The other parameters are $j = 2$, $\Delta t = 0.002$, $\gamma_b = 0.1$ and $N_t = 50$.

5. Summary

In this work, we propose an SNN-based CIM structure and study the dynamics that behave like spiking neurons, which can be realized by injecting the dissipative pulses anti-symmetrically coupled to DOPO pulse on the CIM with MFB. Compared with the conventional CIM, the oscillation region of SNN-based CIM would help the DOPOs to realize the transition between degenerate ground states to search for the optimal spins configuration of the Ising model more efficiently. In addition, we numerically study the variance of CIM and SNN-based CIM. It is found that parametric amplification and de-amplification have alternately existed in the searching process of SNN-CIM, which is different from that of CIM with only parametric amplification. The performance of computation tested on problems with different scales show that the SNN-based CIM has a higher probability of successful solutions than CIM, and introducing a dissipative pulse may improve the computational speed. Furthermore, the study of saturation parameters reveals that the SNN-based CIM is less affected by high saturation parameters, which would help reduce the energy required for the solution [27].

In summary, we propose a new CIM architecture that can be used to solve combinatorial optimization problems and has a higher solution success rate and speed-up effect. Although there have been several methods, such as using squeezed light in the injection light path [45], or using quantum adiabatic theorem to speed up the computing [46,47], our method based on spiking neural network provides an efficient solution which is different from the above methods in improving the calculation success rate and speed up the computing. We believe the SNN-based CIM can bring new paths to quantum-inspired algorithms. And we propose a scheme that uses CIM to implement spiking neurons and can adjust the connection relationship between these neurons through FPGA, which provides a new scheme for the implement of neural computing network.

Optics EXPRESS

Funding. National Natural Science Foundation of China (62131002).

Disclosures. The authors declare no conflicts of interest.

Data availability. No data were generated or analyzed in the presented research.

References

1. E. Farhi, J. Goldstone, S. Gutmann, J. Lapan, A. Lundgren, and D. Preda, "A quantum adiabatic evolution algorithm applied to random instances of an np-complete problem," Science **292**(5516), 472–475 (2001).
2. T. Byrnes, K. Yan, and Y. Yamamoto, "Accelerated optimization problem search using bose–einstein condensation," New J. Phys. **13**(11), 113025 (2011).
3. Z. Wang, A. Marandi, K. Wen, R. L. Byer, and Y. Yamamoto, "Coherent ising machine based on degenerate optical parametric oscillators," Phys. Rev. A **88**(6), 063853 (2013).
4. A. Marandi, Z. Wang, K. Takata, R. L. Byer, and Y. Yamamoto, "Network of time-multiplexed optical parametric oscillators as a coherent ising machine," Nat. Photonics **8**(12), 937–942 (2014).
5. P. L. McMahon, A. Marandi, Y. Haribara, R. Hamerly, C. Langrock, S. Tamate, T. Inagaki, H. Takesue, S. Utsunomiya, K. Aihara, R. L. Byer, M. M. Fejer, H. Mabuchi, and Y. Yamamoto, "A fully programmable 100-spin coherent ising machine with all-to-all connections," Science **354**(6312), 614–617 (2016).
6. T. Inagaki, Y. Haribara, K. Igarashi, T. Sonobe, S. Tamate, T. Honjo, A. Marandi, P. L. McMahon, T. Umeki, K. Enbutsu, O. Tadanaga, H. Takenouchi, K. Aihara, K. ichi Kawarabayashi, K. Inoue, S. Utsunomiya, and H. Takesue, "A coherent ising machine for 2000-node optimization problems," Science **354**(6312), 603–606 (2016).
7. Y. Yamamoto, K. Aihara, T. Leleu, K.-i Kawarabayashi, S. Kako, M. Fejer, K. Inoue, and H. Takesue, "Coherent ising machines—optical neural networks operating at the quantum limit," npj Quantum Inf. **3**(1), 49 (2017).
8. N. Mohseni, P. L. McMahon, and T. Byrnes, "Ising machines as hardware solvers of combinatorial optimization problems," Nat. Rev. Phys. **4**(6), 363–379 (2022).
9. H. Wang, Y. Xue, Y. Qu, X. Mu, and H. Ma, "Multidimensional bose quantum error correction based on neural network decoder," npj Quantum Inf. **8**(1), 134 (2022).
10. R. Hamerly, T. Inagaki, P. L. McMahon, D. Venturelli, A. Marandi, T. Onodera, E. Ng, C. Langrock, K. Inaba, T. Honjo, K. Enbutsu, T. Umeki, R. Kasahara, S. Utsunomiya, S. Kako, K.-I. Kawarabayashi, R. L. Byer, M. M. Fejer, H. Mabuchi, D. Englund, E. Rieffel, H. Takesue, and Y. Yamamoto, "Experimental investigation of performance differences between coherent ising machines and a quantum annealer," Sci. Adv. **5**(5), eaau0823 (2019).
11. S. Utsunomiya, K. Takata, and Y. Yamamoto, "Mapping of ising models onto injection-locked laser systems," Opt. Express **19**(19), 18091–18108 (2011).
12. D. Pierangeli, G. Marcucci, and C. Conti, "Large-scale photonic ising machine by spatial light modulation," Phys. Rev. Lett. **122**(21), 213902 (2019).
13. B. Sutton, K. Y. Camsari, B. Behin-Aein, and S. Datta, "Intrinsic optimization using stochastic nanomagnets," Sci. Rep. **7**(1), 44370 (2017).
14. M. Saccone, F. Caravelli, K. Hofhuis, S. Parchenko, Y. A. Birkhölzer, S. Dhuey, A. Kleibert, S. Van Dijken, C. Nisoli, and A. Farhan, "Direct observation of a dynamical glass transition in a nanomagnetic artificial hopfield network," Nat. Phys. **18**(5), 517–521 (2022).
15. B. Kiraly, E. J. Knol, W. M. van Weerdenburg, H. J. Kappen, and A. A. Khajetoorians, "An atomic boltzmann machine capable of self-adaption," Nat. Nanotechnol. **16**(4), 414–420 (2021).
16. C. Yoshimura, M. Yamaoka, M. Hayashi, T. Okuyama, H. Aoki, K.-i. Kawarabayashi, and H. Mizuno, "Uncertain behaviours of integrated circuits improve computational performance," Sci. Rep. **5**(1), 16213 (2015).
17. T. Inagaki, K. Inaba, R. Hamerly, K. Inoue, Y. Yamamoto, and H. Takesue, "Large-scale ising spin network based on degenerate optical parametric oscillators," Nat. Photonics **10**(6), 415–419 (2016).
18. T. Honjo, T. Sonobe, K. Inaba, T. Inagaki, T. Ikuta, Y. Yamada, T. Kazama, K. Enbutsu, T. Umeki, R. Kasahara, K. ichi Kawarabayashi, and H. Takesue, "100, 000-spin coherent ising machine," Sci. Adv. **7**(40), eabh0952 (2021).
19. T. Ikuta, T. Inagaki, K. Inaba, T. Honjo, T. Kazama, K. Enbutsu, T. Kashiwazaki, R. Kasahara, T. Umeki, and H. Takesue, "Continuous and long-term stabilization of degenerate optical parametric oscillators for large-scale optical hybrid computers," Opt. Express **28**(26), 38553–38566 (2020).
20. K. Inaba, T. Inagaki, K. Igarashi, S. Utsunomiya, T. Honjo, T. Ikuta, K. Enbutsu, T. Umeki, R. Kasahara, K. Inoue, Y. Yamamoto, and H. Takesue, "Potts model solver based on hybrid physical and digital architecture," Commun. Phys. **5**(1), 137 (2022).
21. T. Wang, L. Wu, P. Nobel, and J. Roychowdhury, "Solving combinatorial optimisation problems using oscillator based ising machines," Nat. Comput. **20**(2), 287–306 (2021).
22. K. Kurasawa, K. Hashimoto, A. Li, K. Sato, K. Inaba, H. Takesue, K. Aihara, and M. Hasegawa, "A high-speed channel assignment algorithm for dense ieee 802.11 systems via coherent ising machine," IEEE Wireless Commun. Lett. **10**(8), 1682–1686 (2021).
23. A. K. Singh, K. Jamieson, P. L. McMahon, and D. Venturelli, "Ising machines' dynamics and regularization for near-optimal mimo detection," IEEE Trans. Wireless Commun. **21**(12), 11080–11094 (2022).
24. T. Leleu, Y. Yamamoto, S. Utsunomiya, and K. Aihara, "Combinatorial optimization using dynamical phase transitions in driven-dissipative systems," Phys. Rev. E **95**(2), 022118 (2017).

Optics EXPRESS

25. S. Reifenstein, S. Kako, F. Khoyratee, T. Leleu, and Y. Yamamoto, "Coherent ising machines with optical error correction circuits," Adv. Quantum Technol. **4**(11), 2100077 (2021).
26. T. Leleu, Y. Yamamoto, P. L. McMahon, and K. Aihara, "Destabilization of local minima in analog spin systems by correction of amplitude heterogeneity," Phys. Rev. Lett. **122**(4), 040607 (2019).
27. S. Kako, T. Leleu, Y. Inui, F. Khoyratee, S. Reifenstein, and Y. Yamamoto, "Coherent ising machines with error correction feedback," Adv. Quantum Technol. **3**(11), 2000045 (2020).
28. T. Leleu, F. Khoyratee, T. Levi, R. Hamerly, T. Kohno, and K. Aihara, "Scaling advantage of chaotic amplitude control for high-performance combinatorial optimization," Commun. Phys. **4**(1), 266 (2021).
29. W. Maass, "Networks of spiking neurons: the third generation of neural network models," Neural networks **10**(9), 1659–1671 (1997).
30. R. Brette, M. Rudolph, T. Carnevale, M. Hines, D. Beeman, J. M. Bower, M. Diesmann, A. Morrison, P. H. Goodman, F. C. Harris, M. Zirpe, T. Natschläger, D. Pecevski, B. Ermentrout, M. Djurfeldt, A. Lansner, O. Rochel, T. Vieville, E. Muller, A. P. Davison, S. El Boustani, and A. Destexhe, "Simulation of networks of spiking neurons: a review of tools and strategies," J. Comput. Neurosci. **23**(3), 349–398 (2007).
31. E. M. Izhikevich, "Simple model of spiking neurons," IEEE Trans. Neural Netw. **14**(6), 1569–1572 (2003).
32. V. Mnih, K. Kavukcuoglu, D. Silver, A. A. Rusu, J. Veness, M. G. Bellemare, A. Graves, M. Riedmiller, A. K. Fidjeland, G. Ostrovski, S. Petersen, C. Beattie, A. Sadik, I. Antonoglou, H. King, D. Kumaran, D. Wierstra, S. Legg, and D. Hassabis, "Human-level control through deep reinforcement learning," Nature **518**(7540), 529–533 (2015).
33. Q. Yu, K. C. Tan, and H. Tang, "Pattern recognition computation in a spiking neural network with temporal encoding and learning," in *The 2012 International Joint Conference on Neural Networks (IJCNN)*, (IEEE, 2012), pp. 1–7.
34. T. Inagaki, K. Inaba, T. Leleu, T. Honjo, T. Ikuta, K. Enbutsu, T. Umeki, R. Kasahara, K. Aihara, and H. Takesue, "Collective and synchronous dynamics of photonic spiking neurons," Nat. Commun. **12**(1), 2325 (2021).
35. B. Lu, Y.-P. Gao, K. Wen, and C. Wang, "Combinatorial optimization solving by coherent ising machines based on spiking neural networks," arXiv preprint arXiv:2208.07502 (2022).
36. J. Eisert, S. Scheel, and M. B. Plenio, "Distilling gaussian states with gaussian operations is impossible," Phys. Rev. Lett. **89**(13), 137903 (2002).
37. P. Drummond and C. Gardiner, "Generalised p-representations in quantum optics," J. Phys. A: Math. Gen. **13**(7), 2353–2368 (1980).
38. Y. Inui, M. D. S. H. Gunathilaka, S. Kako, T. Aonishi, and Y. Yamamoto, "Control of amplitude homogeneity in coherent ising machines with artificial zeeman terms," Commun. Phys. **5**(1), 154 (2022).
39. D. Maruo, S. Utsunomiya, and Y. Yamamoto, "Truncated wigner theory of coherent ising machines based on degenerate optical parametric oscillator network," Phys. Scr. **91**(8), 083010 (2016).
40. H. M. Wiseman and G. J. Milburn, "Quantum theory of field-quadrature measurements," Phys. Rev. A **47**(1), 642–662 (1993).
41. W. R. Clements, J. J. Renema, Y. H. Wen, H. M. Chrzanowski, W. S. Kolthammer, and I. A. Walmsley, "Gaussian optical ising machines," Phys. Rev. A **96**(4), 043850 (2017).
42. J. Xiang, Y. Zhang, Y. Zhao, X. Guo, and Y. Su, "All-optical silicon microring spiking neuron," Photonics Res. **10**(4), 939–946 (2022).
43. F. Böhm, T. V. Vaerenbergh, G. Verschaffelt, and G. Van der Sande, "Order-of-magnitude differences in computational performance of analog ising machines induced by the choice of nonlinearity," Commun. Phys. **4**(1), 149 (2021).
44. A. Yamamura, K. Aihara, and Y. Yamamoto, "Quantum model for coherent ising machines: Discrete-time measurement feedback formulation," Phys. Rev. A **96**(5), 053834 (2017).
45. L. Luo, H. Liu, N. Huang, and Z. Wang, "Speed-up coherent ising machine with a squeezed feedback system," Opt. Express **28**(2), 1914–1926 (2020).
46. L. Li, H. Liu, N. Huang, and Z. Wang, "Accuracy-enhanced coherent ising machine using the quantum adiabatic theorem," Opt. Express **29**(12), 18530–18539 (2021).
47. E. S. Tiunov, A. E. Ulanov, and A. Lvovsky, "Annealing by simulating the coherent ising machine," Opt. Express **27**(7), 10288–10295 (2019).